Imaging of goblet cells as a marker for intestinal metaplasia of the stomach by one-photon and two-photon fluorescence endomicroscopy

Hongchun Bao
Swinburne University of Technology
Center for Micro-Photonics
Faculty of Engineering & Industrial Sciences
P.O. Box 218 John Street
Hawthorn, Victoria 3122
Australia

Alex Boussioutas
Research-Peter MacCallum Cancer Centre
1 St. Andrews Place
East Melbourne, Victoria 3002
Australia
and
University of Melbourne
Western Hospital
Department of Medicine (RMH/WH)
Footscray, 3011
Australia

Jeremy Reynolds
Research-Peter MacCallum Cancer Centre
1 St. Andrews Place
East Melbourne, Victoria 3002
Australia

Sarah Russell
Swinburne University of Technology
Center for Micro-Photonics
Faculty of Engineering & Industrial Sciences
P.O. Box 218 John Street
Hawthorn, Victoria 3122
Australia
and
Research-Peter MacCallum Cancer Centre
1 St. Andrews Place
East Melbourne, Victoria 3002
Australia

Min Gu
Swinburne University of Technology
Center for Micro-Photonics
Faculty of Engineering & Industrial Sciences
P.O. Box 218 John Street
Hawthorn, Victoria 3122
Australia

Abstract. Goblet cells are a requirement for the diagnosis of intestinal metaplasia of the stomach. The gastric mucosa is lined by a monolayer of columnar epithelium with some specialization at the crypts, but there are no goblet cells in normal gastric epithelium. The appearance of goblet cells in gastric epithelium is an indicator of potential malignant progression toward adenocarcinoma. Therefore, *in vivo* three-dimensional imaging of goblet cells is essential for diagnoses of a premalignant stage of gastric cancers called intestinal metaplasia. We used mouse intestine, which has goblet cells, as a model of intestinal metaplasia. One-photon confocal fluorescence endomicroscopy and two-photon fluorescence endomicroscopy are employed for 3-D imaging of goblet cells. The penetration depth, the sectioning ability, and the photobleaching information of imaging are demonstrated. Both endomicroscopy techniques can three-dimensionally observe goblet cells in mouse large intestine and achieve an imaging depth of 176 μm. The two-photon fluorescence endomicroscopy shows higher resolution and contrast of the imaging sections at each depth. In addition, two-photon fluorescence endomicroscopy also has advantages of sectioning ability and less photobleaching. These results prove that two-photon fluorescence endomicroscopy is advantageous in diagnoses of a premalignant stage of gastric cancers. [DOI: 10.1117/1.3269681]

Keywords: endomicroscopy; two-photon fluorescence imaging; one-photon fluorescence imaging; gastrointestinal cancers; goblet cells.

Paper 09160RR received May 3, 2009; revised manuscript received Oct. 1, 2009; accepted for publication Oct. 13, 2009; published online Dec. 7, 2009.

Endomicroscopy, which has a miniaturized probe, can be guided through a human gastrointestinal tract and view gross cell structures of internal organs. The technology is an important progression in the armamentarium for detecting gastrointestinal cancers at an early stage.[1–3] It is envisioned that real-time *in vivo* endomicroscopy will allow clinicians to detect otherwise undetectable gastrointestinal tract lesions by standard white-light endoscopy and allow precise targeting for biopsy. It is notable that there are limitations with current biopsy due to artifacts introduced by the biopsy procedure that could be overcome with real-time endomicroscopy.[4–6]

Address all correspondence to: Min Gu, Center for Micro-Photonics, Faculty of Engineering & Industrial Sciences, Swinburne University of Technology, Hawthorn, Victoria 3122, Australia. Tel: 61-3-92148776; Fax: 61-3-92145435; E-mail: mgu@swin.edu.au

1083-3668/2009/14(6)/064031/4/$25.00 © 2009 SPIE

Correa hypothesized that intestinal metaplasia of the stomach is a premalignant lesion of gastric cancer and that this would be the earliest indicator of potential malignant progression to gastric cancer.[7,8] A histopathological criterion of intestinal metaplasia is the presence of goblet cells. Goblet cells are normally found in the epithelial layer of the colon and intestine but not in the normal stomach. The occurrence of goblet cells in the columnar epithelium of the stomach is pathognomonic for intestinal metaplasia.[7,8] The capability of endomicroscopy to three-dimensionally image goblet cells is important for the detection of early lesions, which would allow patients to be enrolled in screening programs for the early detection of gastric cancer. Here, we use mouse intestine as a model of intestinal metaplasia due to the presence of many goblet cells.

In this letter, one-photon confocal fluorescence endomicroscopy (OPFE) and two-photon fluorescence endomicroscopy (TPFE) are employed for 3-D imaging of goblet cells. The penetration depth, the sectioning ability, and the photobleaching information of imaging are demonstrated to show the capability of OPFE and TPFE in 3-D imaging of goblet cells for diagnoses of a premalignant stage of gastric cancers.

The OPFE system (FIVE, Optiscan Pty. Ltd.) uses a single-mode fiber coupler to deliver 488-nm continuous-wave (CW) laser beam to a sample and collect the one-photon excited fluorescence signal for imaging. The OPFE system is a confocal microscopy system where the core of the single-mode fiber acts as a pinhole. This OPFE has been used for 3-D viewing of human and mouse gastrointestinal system *in vivo* and for differentiating epithelial gaps and goblet cells.[9,10] The TPFE system employs a length of double-clad fiber (DCF) to deliver near-inftrared (NIR) laser pulses to a sample and collect two-photon-excited fluorescence signal through the inner cladding of the DCF for imaging.[11] This TPFE device has been applied for fast and clear 3-D imaging of animal tissues with a large field of view,[11] which cannot be achieved by other TPFE geometry.[12–23]

Fluorescein is soluble in water and safe to be used in humans. The body's vascular system carries fluorescein to the whole body. Fluorescein is absorbed by epithelial cells from the bloodstream. Most cells will then be visualized due to fluorescein in their cytoplasm. Goblet cells are seen as dark ovoid structures due to the mucin contained in their cytoplasm that displaces the fluorescein. The 3-D imaging of goblet cells by OPFE and TPFE was performed after a mouse was injected with fluorescein intravenously. The excitation wavelength for TPFE imaging is 790 nm, which is the wavelength at the peak of the two-photon excitation spectrum of fluorescein. Figures 1(a1) to 1(b5) display 3-D OPFE and TPFE images of the same part of a mouse large intestine up to 176 μm deep. Figures 1(a1) and 1(b1) are the surface images of the mouse intestine by OPFE and TPFE. Both endomicroscopy techniques show clear surface images of the mouse intestine. However, the surface image obtained by TPFE has much more goblet cells (dark dots) than that from OPFE. The resolution and contrast of the TPFE imaging are higher than those of OPFE imaging. At a depth of 44 μm under the mouse intestine surface, the section image from TPFE still displays clear goblet cells, as shown in Fig. 1(b2), while the section image from OPFE can hardly identify the goblet cells.

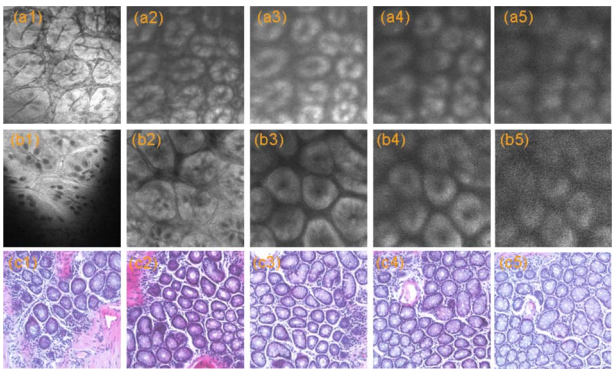

Fig. 1 OPFE images of goblet cells at (a1) surface, (a2) 44 μm, (a3) 88 μm, (a4) 132 μm, and (a5) 176 μm under the mouse intestine epithelium. TPFE images of goblet cells at (b1) surface, (b2) 44 μm, (b3) 88 μm, (b4) 132 μm, and (b5) 176 μm under the mouse intestine epithelium. Histological images of the mouse large intestine at (c1) surface, (c2) 44 μm, (c3) 88 μm, (c4) 132 μm, and (c5) 176 μm under the mouse intestine epithelium. (a1) to (a5); (b1) to (b5) Size of the images: 200 μm $\times$ 200 μm. (c1) to (c5) Size of the images: 550 μm $\times$ 550 μm.

At 88 μm deep, TPFE shows the sharp gland structure of the mouse intestine and goblet cells in the gland, as shown in Fig. 1(b3). On the other hand, the structure of the gland in the OPFE section image, as shown in Fig. 1(a3), becomes blurred and no goblet cell can be identified in the gland. The gland structure of TPFE imaging starts to be blurred at 132 μm deep, as displayed in Fig. 1(b4), but is still clearer than the OPFE image, as shown in Fig. 1(a4). At 176 μm deep, the gland structure can still be identified in the section image from TPFE, as illustrated in Fig. 1(b5), while it can not be observed in the section image from OPFE, as shown in Fig. 1(a5). In OPFE and TPFE imaging, both unscattered and scattered illumination photons can contribute to fluorescence emission. However, two-photon fluorescence produced by the scattered illumination photons exhibits a lower signal level than one-photon fluorescence. The stronger suppression of the contributions from scattered illumination offers TPFE an advantage in image resolution.[24] The histological images of the mouse large intestine at surface, 44 μm, 88 μm, 132 μm, and 176 μm under the mouse intestine epithelium are shown in Figs. 1(c1) to 1(c5). The images display a similar gland structure. However, goblet cells are difficult to identify from the histological images.

For 3-D imaging, the image sectioning mechanism of the OPFE and TPFE systems is different.[14–16] The OPFE system uses the core of a fiber as a pinhole to block the fluorescence signal coming from the out-of-focus region to realize section imaging. The size of the core of the fiber determines how thin each section can be. Here, the mode field diameter of the fiber OPFE usesd is 5.3 μm. On the other hand, the TPFE system is based on nonlinear processes, and fluorescence can generate only at the focal spot where it has a high power density. How thin each section of image can be is determined by the focus spot size along the axial direction. The numerical aperture (NA) of TPFE is 0.35. The lens in TPFE accurately corrects image aberration and realizes a diffraction-limited focus spot.[11]

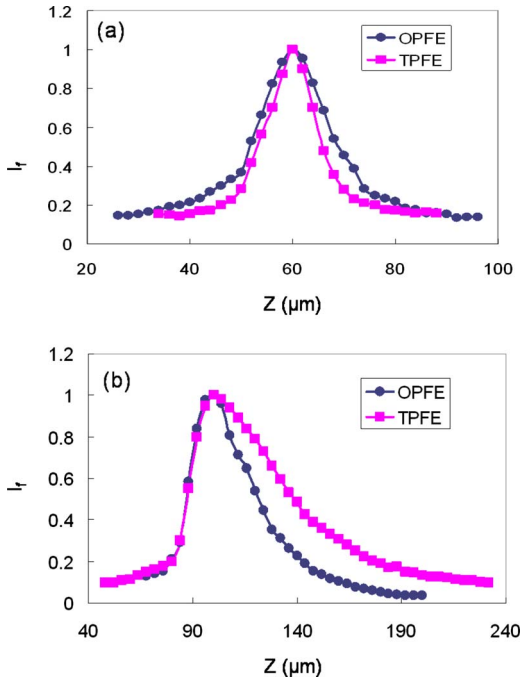

Fig. 2 (a) Axial response of a thin layer of DABM dye by OPFE and TPFE. (b) Axial response of thick mouse intestine tissue by OPFE and TPFE.

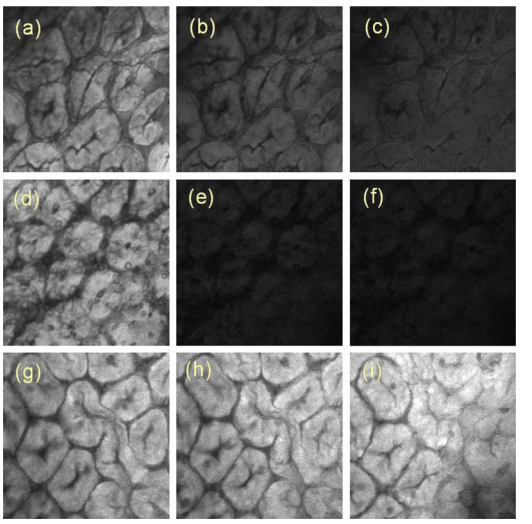

Fig. 3 OPFE image of the mouse intestine with 220-μW power on the sample. (a) First scan; (b) scanned for 5 min; and (c) scanned for 10 min. OPFE image of the mouse intestine with 440-μW power on the sample. (d) First scan; (e) scanned for 5 min; and (f) has been scanned for 10 min. TPFE image of the mouse intestine with 38-mW power on the sample. (g) First scan; (h) scanned for 5 min; and (i) scanned for 10 min. Size of the images: 200 μm $\times$ 200 μm.

To compare the optical sectioning ability of OPFE and TPFE, we measure their axial response of a thin layer of 4-diethylaminobenzylidene-malononitrile (DABM) dye, as shown in Fig. 2(a). The results are averages of 10 independent measurements. TPFE shows a narrower axial response than that of OPFE. The full width at half maximum (FWHM) of the intensity profile for TPFE and OPFE is 10 μm and 14 μm, respectively. Therefore TPFE has a higher sectioning ability.

On the other hand, the axial response of a layer of thick mouse intestine tissue ($>$2 mm) by the TPFE system and the OPFE system is different. Figure 2(b) displays the axial response of a thick layer of mouse intestine by TPFE and OPFE. The mouse intestine tissue was harvested from the mouse immediately after it was injected with fluorescein intravenously (tail vein injection). The optical power on the tissue for TPFE and OPFE is 30 mW and 20 μW. As shown in Fig. 2(b), the left side from the peak of the response curve is the fluorescence response from the top of the murine intestinal epithelium by TPFE and OPFE, where TPFE and OPFE show similar responses. The right side from the peak of the response curve in Fig. 2(b) is the fluorescence response from the underneath of the murine intestinal epithelium by TPFE and OPFE, where TPFE has higher fluorescence intensity at each depth under the murine intestinal epithelium. Because the 790-nm excitation laser beam that TPFE uses suffers less loss from the absorption and Rayleigh scattering than that of the 488-nm excitation laser beam that OPFE uses, the dropping of the TPFE signal is slower than that of the OPFE signal under the murine intestinal epithelium.

In addition, TPFE also shows less photobleaching during imaging. Figure 3 shows the OPFE and TPFE images of the mouse intestine at first scanning, after scanning for 5 min, and after scanning for 10 min. Figures 3(a)–3(c) are the OPFE images where the excitation laser power to the mouse intestine is 220 μW. Compared with Fig. 3(a), Figs. 3(b) and 3(c) become obviously darker. The exposure of the excitation laser beam on the mouse intestine causes photobleaching of the fluorescein, and thus the OPFE images of the intestine become darker. The OPFE image of the mouse intestine after scanning for 10 min, as displayed in Fig. 3(c), is darker than that after scanning for 5 min, as shown in Fig. 3(b). The longer the exposure time, the more severerly the OPFE system suffers from photobleaching. Figures 3(d)–3(f) are the OPFE images of the mouse intestine while the excitation laser power is 440 μW. Comparing with Figs. 3(a)–3(c), the OPFE images become darker with the increase of the excitation laser power for the same scanning time. Therefore, the high excitation laser power causes high photobleaching in OPFE imaging. On the other hand, the brightness of TPFE images, as shown in Figs. 3(g)–3(i), does not show an obvious change after scanning for 5 and 10 min, even if the excitation laser power is at the maximum of the TPFE output power of 38 mW. Therefore, TPFE imaging has much less photobleaching than OPFE imaging.

The fluorescence intensity of OPFE and TPFE images after different numbers of scans is measured. Figure 4 is the normalized fluorescence intensity of OPFE and TPFE images (normalized to the peak fluorescence intensity) after different numbers of scanning. As shown in Fig. 4, the fluorescence intensity of the OPFE images drops quickly after scanning. After 208 scan times, the fluorescence intensity of the OPFE image is half that in the first scan if the excitation laser power is 220 μW. As the excitation laser power increases to 220 μW, it takes only 126 scan times-for the fluorescence intensity of the OPFE image to become half of that in the first scan. Alternatively, the fluorescence intensity of the TPFE im-

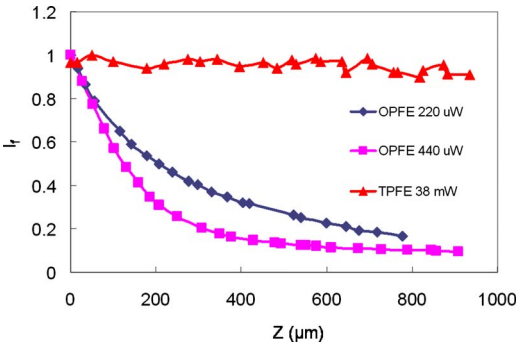

Fig. 4 Normalized fluorescence intensity versus number of scans.

age is stable even when the excitation laser power is at the maximum of the TPFE output power of 38 mW and the sample has been scanned for 900 scan times. The fluorescence intensity and the photobleaching rate for OPFE have a linear dependence on the excitation laser power. On the other hand, the fluorescence intensity for TPFE is dependent on the square of the excitation laser power, and the photobleaching rate is dependent on the cube of the excitation laser power.[25] Therefore, TPFE is less efficient in generating fluorescence and even less effective in photobleaching.

In summary, the capacity of OPFE and TPFE for 3-D imaging of goblet cells is necessary for them to be utilized in early diagnoses of gastric cancers. First, experiments reveal that both OPFE and TPFE can achieve 176-μm penetration depths in 3-D imaging. However, TPFE shows higher resolution and contrast of the sectioned image at different depths. Second, TPFE has higher sectioning ability than that of OPFE. If the excitation power is fixed, TPFE shows a larger penetration depth. Third, although TPFE uses a higher power of excitation light, TPFE shows much less photobleaching and photodamaging to mouse intestine even with power more than 170 times higher than that of OPFE. Therefore, for diagnoses of a premalignant stage of gastric cancers, TPFE has shown more advantages than OPFE.

The authors thank the Australian Research Council for its support and Optiscan Pty. Ltd. for providing FIVE1 one-photon fluorescence endomicroscopy and supporting the setup of two-photon fluorescence endomicroscopy.

References

1. W. Denk, J. H. Strickler, and W. W. Webb, "Two-photon laser scanning fluorescence microscopy," *Science* **248**, 73–76 (1990).
2. K. Konig, A. Ethlers, I. Riemann, S. Schenkl, R. Buckle, and M. Kaatz, "Clinical two-photon microendoscopy," *Microsc. Res. Tech.* **70**, 398–402 (2007).
3. Y. Kakeji, S. Yamaguchi, D. Yoshida, K. Tanoue, M. Ueda, A. Masunari, T. Utsunomiya, M. Imamura, H. Honda, Y. Maehara, and M. Hashizume, "Development and assessment of morphologic criteria for diagnosing gastric cancer using confocal endomicroscopy: an *ex vivo* and *in vivo* study," *Endoscopy* **38**, 886–890 (2006).
4. N. Muguruma1 and S. Ito, "Endoscopic molecular imaging: beacon to the destination," *Dig. Endosc.* **20**, 101–106 (2008).
5. V. Nadeau, M. Padgett, J. Hewett, W. Sibbett, K. Hamdan, S. Mohammed, I. Tait, and A. Cushieri, "A compact endoscopic fluorescence detection system for gastrointestinal cancers," *Proc. SPIE* **4248**, 91–96 (2001).
6. B. A. Flusberg, E. D. Cocker, W. Piyawattanametha, J. C. Jung, E. L. M. Cheung, and M. J. Schnitzer, "Fiber-optic fluorescence imaging," *Nat. Methods* **2**, 941–944 (2005).
7. R. Kiesslich, P. R. Galle, and M. F. Neurath, *Atlas of Endomicroscopy*, Springer Medizin Verlag, Heidelberg (2008).
8. P. Correa, "Human gastric carcinogenesis: a multistep and multifactorial process—first American Cancer Society award lecture on cancer epidemiology and prevention," *Cancer Res.* **53**, 6735–6740 (1992).
9. R. Kiesslich, M. Goetz, E. M. Angus, Q. Hu, Y. Guan, C. Potten, T. Allen, M. F. Neurath, N. F. Shroyer, M. H. Montrose, and A. J. M. Watson, "Identification of epithelial gaps in human small and large intestine by confocal endomicroscopy," *Gastroenterology* **133**, 1769–1778 (2007).
10. I. Odagi, T. Kato, H. Imazu, M. Kaise, S. Omar, and H. Tajiri, "Examination of normal intestine using confocal endomicroscopy," *J. Gastroenterol. Hepatol* **22**, 658–662 (2007).
11. H. Bao, J. Allen, R. Pattie, R. Vance, and M. Gu, "A fast handhold two-photon fluorescence micro-endoscope with a 475 μm×475 μm field of view for *in vivo* imaging," *Opt. Lett.* **33**, 1333–1335 (2008).
12. L. Fu, A. Jain, C. Cranfield, H. Xie, and M. Gu, "Three-dimensional nonlinear optical endoscopy," *J. Biomed. Opt.* **12**, 040501 (2007).
13. L. Fu, X. Gan, and M. Gu, "Nonlinear optical microscopy based on double-clad photonic crystal fibers," *Opt. Express* **13**, 5528–5534 (2005).
14. L. Fu, A. Jain, H. Xie, C. Cranfield, and M. Gu, "Nonlinear optical endoscopy based on a double-clad photonic crystal fiber and a MEMS mirror," *Opt. Express* **14**, 1027–1032 (2006).
15. L. Fu and M. Gu, "Fiber-optic nonlinear optical microscopy and endoscopy," *J. Microsc.* **226**, 195–206 (2007).
16. D. Bird and M. Gu, "Compact two-photon fluorescence microscope based on a single-mode fiber coupler," *Opt. Lett.* **27**, 1031–1033 (2002).
17. D. Bird and M. Gu, "Two-photon fluorescence endoscopy with a micro-optic scanning head," *Opt. Lett.* **28**, 1552–1554 (2003).
18. D. Bird and M. Gu, "Fiber-optic two-photon scanning fluorescence microscopy," *J. Microsc.* **208**, 35–48 (2002).
19. H. Bao and M. Gu, "Reduction of self-phase modulation in double-clad photonic crystal fiber for nonlinear optical endoscopy," *Opt. Lett.* **34**, 148–150 (2009).
20. W. Jung, S. Tang, D. T. McCormic, T. Xie, Y. C. Ahn, J. Su, I. V. Tomov, T. B. Krasieva, B. J. Tromberg, and Z. Chen, "Miniaturized probe based on a microelectromechanical system mirror for multiphoton microscopy," *Opt. Lett.* **33**, 1324–1326 (2008).
21. C. L. Hoy, N. J. Durr, P. Chen, W. Piyawattanametha, H. Ra, O. Solgaard, and A. Ben-Yakar, "Miniaturized probe for femtosecond laser microsurgery and two-photon imaging," *Opt. Express* **16**, 9996–10005 (2008).
22. M. Goetz, C. Fottner, E. Schirrmacher, P. Delaney, S. Gregor, C. Schneider, D. Strand, S. Kanzler, B. Memadathil, E. Weyand, M. Holtmann, R. Schirrmacher, M. M. Weber, M. Anlauf, G. Klöppel, M. Vieth, P. R. Galle, P. Bartenstein, M. F. Neurath, and R. Kiesslich, "*In vivo* confocal real-time mini-microscopy in animal models of human inflammatory and neoplastic diseases," *Endoscopy* **39**, 350–356 (2007).
23. M. T. Myaing, D. J. MacDonald, and X. Li, "Fiber-optic scanning two-photon fluorescence endoscope," *Opt. Lett.* **31**, 1076–1078 (2006).
24. M. Gu, X. Gan, A. Kisteman, and M. G. Xu, "Comparison of penetration depth between two-photon excitation and single-photon excitation in imaging through turbid tissue media," *Appl. Phys. Lett.* **77**, 1551–1553 (2000).
25. G. H. Patterson and D. W. Piston, "Photobleaching in two-photon excitation microscopy," *Biophys. J.* **78**, 2159–2162 (2000).